Journal of
Applied
Crystallography
ISSN 0021-8898

Received 7 August 2000
Accepted 16 January 2001

Treatment of grazing-incidence small-angle X-ray scattering data taken above the critical angle

A. Martorana,[a,b]* A Longo,[b] F. d'Acapito,[c] C. Maurizio,[d] E. Cattaruzza[e] and F. Gonella[e]

[a]Dipartimento di Chimica Inorganica, Università di Palermo, Viale delle Scienze, I-90128 Palermo, Italy, [b]ICTPN-CNR, via Ugo La Malfa, 153, I-90146 Palermo, Italy, [c]INFM and European Synchrotron Radiation Facility, GILDA-CRG, BP 220, F-38043 Grenoble, France, [d]INFM and Dipartimento di Fisica, Università di Padova, via Marzolo, 8, I-35131, Padova, Italy, and [e]INFM and Dipartimento di Chimica Fisica, Università di Venezia, Dorsoduro 2137, I-30123 Venezia, Italy. Correspondence e-mail: nino@ictpn.pa.cnr.it

The equations taking into account refraction at the sample surface in grazing-incidence small-angle X-ray scattering (GISAXS) when the angle between the incoming beam and the sample surface is slightly larger than the critical angle are derived and discussed. It is demonstrated that the refraction of both the incoming and the scattered beam at the sample surface affects the GISAXS pattern and that, when a planar bidimensional detector perpendicular to the incoming beam is used, the effect depends on the azimuthal detector angle. The smearing of the pattern depending on the size of the illuminated sample area in grazing incidence is estimated by simulations with Cauchy functions of different widths. The possibility of integrating the recorded intensities over a suitable azimuthal angular range and then of making the correction for refraction is also analysed, employing simulations involving the intensity function of mono-disperse interacting hard spheres. As a case study, the refraction correction is applied to the investigation of a Cu–Ni implant on silica glass.

© 2001 International Union of Crystallography
Printed in Great Britain – all rights reserved

1. Introduction

Grazing-incidence small-angle X-ray scattering (GISAXS) (Levine *et al.*, 1989) is a powerful tool for the structural characterization of thin (micrometre scale) superficial layers containing nanosized particles. Samples can be obtained by ion implantation (Babonneau *et al.*, 1999; d'Acapito *et al.*, 1998; Cattaruzza *et al.*, 2000), sol–gel synthesis (Kutsch *et al.*, 1997) or vapour deposition (Naudon & Thiaudière, 1997). Investigation of particles deposited on the surface is usually performed at the critical angle α_c; however, when dealing with buried nanostructures, the working angle must be slightly higher than α_c to permit a controlled limited beam penetration in the matrix. In the latter geometry, the refracted beam acts as the effective primary beam of the SAXS experiment and the scattered radiation is likewise refracted on leaving the sample. Thus, correction is required in order to retrieve the actual scattering angle $2\theta'$ from the measured 2θ between the incoming beam and the outgoing X-rays.

The use of an experimental setup consisting of a planar detector perpendicular to the incident beam assures better counting statistics, with respect to linear devices, and also allows the investigation of anisotropic implants (Babonneau *et al.*, 1999). On the other hand, the scattered beams recorded at the same 2θ but at various azimuthal φ angles strike the sample surface with different inclination, thus requiring suitable correction for refraction. In the literature, the correction is given only on the plane containing the incoming beam and the surface normal of the sample, that is, at $\varphi = 0$ (Kutsch *et al.*, 1997). The equations allowing one to obtain the internal angles $(2\theta', \varphi')$ from the detector angles $(2\theta, \varphi)$ are derived in the next section of this paper.

Despite the small vertical size of the incident beam, its projection on the sample surface is very long when working in grazing incidence (typically a few centimetres), so that the limits of the illuminated sample region are actually determined by the overall sample length. The smearing of the recorded pattern arising from the sample size increases with the scattering angle (becoming noteworthy in the wide-angle region) and decreases with the distance of the sample from the detector element. An estimate of the extent that refraction and sample smearing can affect a pattern recorded under grazing-angle geometry has been achieved by simulations ranging from small to wide X-ray

scattering angles and involving Cauchy functions of different widths.

In principle, the equations taking into account the refraction effect should be applied to every $(2\theta, \varphi)$ pair of detector angles. However, it is shown by simulations involving the scattering intensity of monodisperse interacting hard spheres (Guinier & Fournet, 1955) that for isotropic implants a simplified procedure is allowed, consisting first of azimuthal integration of the recorded intensities and then correction for refraction according to an average φ angle. An application to the actual case of a Cu–Ni-implanted layer on silica glass is also described.

2. Refraction correction

The correction for refraction at the sample surface of both the incident and the scattered beams is based on the scheme drawn in Fig. 1. The angles $(2\theta, \varphi)$ are measured at the detector, whereas $(2\theta', \varphi')$, the actual scattering angles, are referred to a virtual detector placed within the implanted layer and perpendicular to the refracted incoming beam. The equations for the determination of $(2\theta', \varphi')$ are based on Snell's law and on three-dimensional trigonometry:

$$\cos(\alpha') = \cos(\alpha)/(1 - \delta), \tag{1}$$

$$\sin(\sigma) = \cos(\alpha)\sin(2\theta)\cos(\varphi) - \sin(\alpha)\cos(2\theta), \tag{2}$$

$$\cos(\sigma') = \cos(\sigma)/(1 - \delta), \tag{3}$$

$$\cos(\chi) = [\cos(2\theta) + \sin(\alpha)\sin(\sigma)]/\cos(\alpha)\cos(\sigma), \tag{4}$$

$$\cos(2\theta') = \cos(\alpha')\cos(\sigma')\cos(\chi) - \sin(\alpha')\sin(\sigma'), \tag{5}$$

$$\cos(\varphi') = [\sin(\sigma') + \sin(\alpha')\cos(2\theta')]/[\cos(\alpha')\sin(2\theta')], \tag{6}$$

where $(1 - \delta)$ is the real part of the refractive index.

In Fig. 2, the values of $\Delta Q/Q$ [$Q = (4\pi\sin\theta)/\lambda$, $Q' = (4\pi\sin\theta')/\lambda$, $\Delta Q = Q - Q'$] are drawn as a function of the detector angle 2θ, for the α, δ and λ values ($\alpha = 0.25°$, $\delta = 7.7 \times 10^{-6}$, λ = 1.49 Å) of a previously reported experiment (Cattaruzza *et al.*, 2000). From inspection of Fig. 2, the $\Delta 2\theta$ correction is seen to be slightly dependent on φ and more effective at the smaller 2θ values; it is negative (that is, $2\theta' = 2\theta - |\Delta 2\theta|$) and decreases in absolute value with 2θ, whereas the correction concerning the azimuthal angle φ is positive, decreasing with 2θ and increasing with φ. This behaviour can be understood qualitatively by inspection of Fig. 1. The correction for refraction of the scattered beam can be regarded, on the detector plate, as a shift parallel to $-\mathbf{n}_{\rm surf}$ of the intensity recorded at a given pixel. On a fixed scattering ring (that is, at constant 2θ) the shift at $\varphi = 0$ concerns only 2θ, whereas at increasing φ values it tends to become tangential to the scattering ring, thus giving rise to increasing $|\Delta\varphi|$ and decreasing $|\Delta 2\theta|$ values.

From equations (1)–(6), the path $p(2\theta, \varphi)$ within the sample of a scattered beam generated at depth z and detected at $(2\theta, \varphi)$ can be easily calculated as

$$p(2\theta, \varphi) = z/\sin(\sigma'), \tag{7}$$

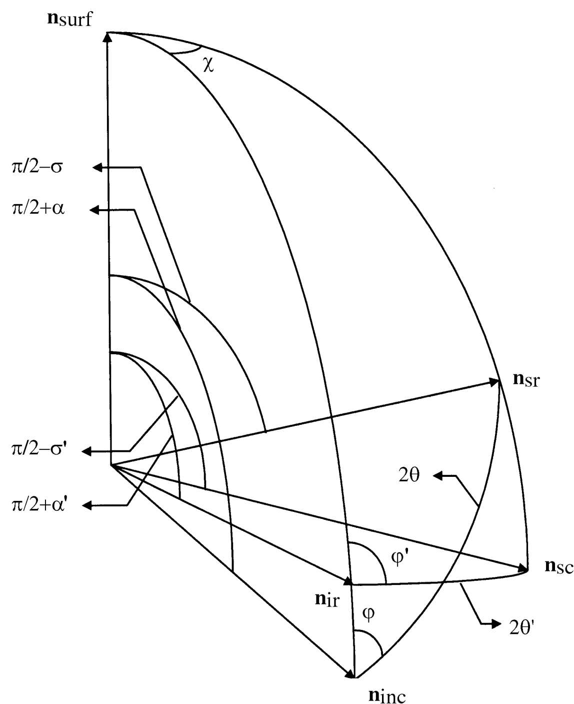

Figure 1
Scheme of directions and angles for refraction correction. $\mathbf{n}_{\rm surf}$ is the unit vector normal to the sample surface; $\mathbf{n}_{\rm inc}$ is the unit vector in the direction of the incoming beam; $\mathbf{n}_{\rm ir}$ is the unit vector in the direction of the refracted incoming beam; $\mathbf{n}_{\rm sc}$ is the unit vector in the direction of the scattered beam; $\mathbf{n}_{\rm sr}$ is the unit vector in the direction of the refracted scattered beam; χ is the angle between the planes ($\mathbf{n}_{\rm surf}$, $\mathbf{n}_{\rm inc}$) and ($\mathbf{n}_{\rm surf}$, $\mathbf{n}_{\rm sc}$); 2θ is the angle between $\mathbf{n}_{\rm inc}$ and $\mathbf{n}_{\rm sr}$, measured at the detector; $2\theta'$ is the scattering angle between $\mathbf{n}_{\rm ir}$ and $\mathbf{n}_{\rm sc}$; α and α' are the angles of the incoming beam at the sample surface before and after refraction, respectively (notice that the angle $\pi/2 + \alpha$ is evaluated between the positive directions of $\mathbf{n}_{\rm surf}$ and $\mathbf{n}_{\rm inc}$, so that the incoming beam actually strikes the sample travelling from left to right in the figure); σ' and σ are the angles of the scattered beam at the sample surface before and after refraction, respectively; φ is the azimuthal detector angle between the planes ($\mathbf{n}_{\rm surf}$, $\mathbf{n}_{\rm inc}$) and ($\mathbf{n}_{\rm inc}$, $\mathbf{n}_{\rm sr}$); φ' is the azimuthal scattering angle between the planes ($\mathbf{n}_{\rm surf}$, $\mathbf{n}_{\rm ir}$) and ($\mathbf{n}_{\rm ir}$, $\mathbf{n}_{\rm sc}$). The angles of the drawing are not to scale, but the relations between them are in agreement with equations (1)–(6): $0 < \alpha' < \alpha$, $0 < \sigma' < \sigma$, $2\theta' < 2\theta$, $\varphi < \varphi'$.

allowing the estimation of the correction for absorption of the transmitted intensity without the approximation $\varphi' \simeq \varphi$ (Kutsch *et al.*, 1997).

3. Smearing effects and simulations

Equations (5) and (6) are valid under the assumption that the illuminated sample has negligible size, so that unique $(2\theta, \varphi)$ angles can be defined at each detector pixel. Whereas the condition on φ is, to a fairly good approximation, fulfilled by the narrow cross section of the incoming beam used for grazing-incidence experiments, the 2θ values may be subject to an uncertainty increasing with 2θ and decreasing with the distance of the detector element from the sample. A scheme of the experimental setup is shown in Fig. 3.

A normalized Cauchy function,

$$I_0(2\theta') = 2\gamma/\{\gamma^2 + [2\pi(2\theta' - 2\theta'_0)]^2\}, \tag{8}$$

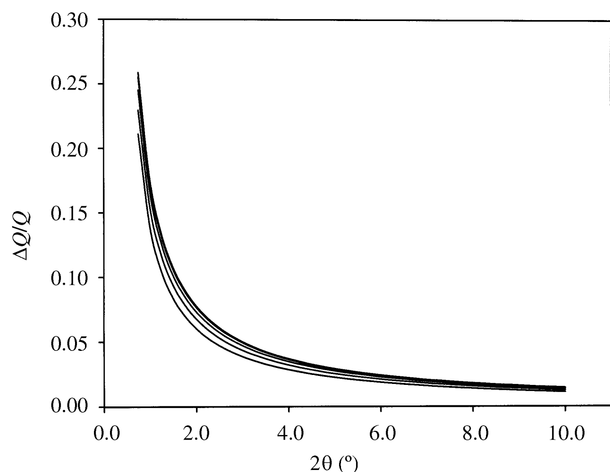

Figure 2
$\Delta Q/Q$, as a function of the detector angle 2θ, for the GISAXS parameters: $\alpha = 0.25°$, $\delta = 7.7 \times 10^{-6}$, $\lambda = 1.49$ Å. The different curves, going downwards from the topmost, are relative to $\varphi = 0$, 10, 20, 30 and 40°.

was used to estimate the influence of the size of the illuminated area on the uncertainty of 2θ. This function, although not related to any actual SAXS application, can be subjected to rigid translation and, therefore, retaining a constant shape, can account for the mere smearing effects at different glancing angles. The grazing incidence patterns were calculated for the above-reported α, δ and λ parameters, for $\varphi = 0$ and for several $2\theta'_0$ values ranging from the small- to the wide-angle region. Different values of γ, varying from 0.25 to 1°, were used to investigate the dependence of the smearing effects on the degree of sharpness of the scattering profile.

The smearing integral,

$$I_{\rm sm}(2\theta) = \int\limits_{-L/2}^{L/2} {\rm d}x\, I[2\theta'(x)], \qquad (9)$$

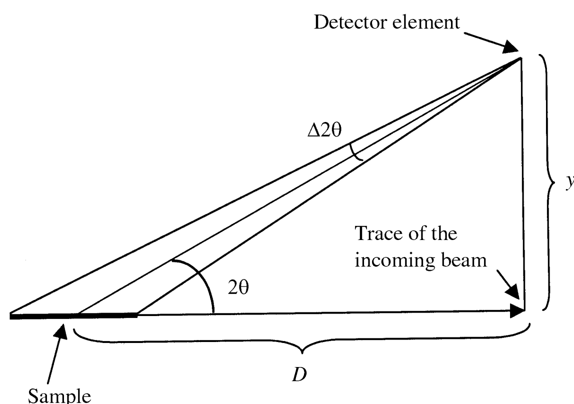

Figure 3
Scheme of the GISAXS experimental setup. D is the distance from the centre of the illuminated sample to the detector; y is the distance of the pixel from the trace of the incoming beam. The small angle α (some tenths of a degree, in grazing-incidence geometry) between the incoming beam and the sample surface is approximated as $\alpha = 0°$, so that in the drawing the sample surface is parallel to the incoming beam.

is calculated by Gaussian quadrature. The integration range is relative to an illuminated sample region of width $L = 10$ mm. According to Fig. 3, the glancing angle $2\theta(x)$ for the element x is given by

$$2\theta(x) = a\tan[y/(D + x)], \qquad (10)$$

where $y = D\tan(2\theta)$, $2\theta \equiv 2\theta(0)$ and $D = 500$ mm; $2\theta'(x)$ in equation (9) is then obtained from $2\theta(x)$ by equation (5). The approximation introduced in equation (10) by ignoring the angle of grazing incidence of the incoming beam with the sample surface is negligible. At first glance, the smeared profiles obtained by equation (9) are indistinguishable from the unsmeared ones for $2\theta < 3°$, whatever the value of γ, whereas the Cauchy functions, in particular the sharpest ones, are severely distorted in the wide-angle region.

Because of the faint dependence of $\Delta 2\theta$ on φ, an effective procedure seems to be, for suitable φ intervals and isotropic implants, first to integrate the two-dimensional detector intensity values over φ and then to perform the correction on 2θ. Possible smearing effects are estimated in the following simulation. The function

$$I_0(Q') = \psi^2(Q'R)/[1 + (8V_0/V_1)\psi(2Q'R)], \qquad (11)$$

proportional to the scattering intensity of monodispersed interacting hard spheres (Guinier & Fournet 1955), is taken into account; R is the particle radius, V_0 its volume, V_1 the volume per particle, and

$$\psi(t) = 3[\sin(t) - t\cos(t)]/t^3. \qquad (12)$$

The smearing integral (9) is calculated as a function of φ; a further integration on φ corresponds to summing the 'observed' intensity values on pixels equidistant from the trace of the direct beam on the detector. In Fig. 4, two sets of simulated data are drawn, relative to $R_1 = 30$ and $R_2 = 60$ Å, respectively. The other parameters are $(8V_0/V_1) = 4$ for both the calculated patterns, $L = 10$ mm, $D = 500$ mm and $\varphi_{\rm min} = 10°$, $\varphi_{\rm max} = 26.5°$; the choice of $\varphi_{\rm min}$, $\varphi_{\rm max}$ depends, as will be discussed on the next section, on actual experimental limitations. Furthermore, a fitting to the 'data' of the unsmeared intensity has been performed, taking into account the refraction effects for $\varphi_{\rm av} = 18°$ and refining an overall scale factor, the particle radius R and the packing factor $(8V_0/V_1)$. From inspection of Fig. 4, it is evident that only on a logarithmic intensity scale can some difference be appreciated between the simulated data and the fitted pattern; the broader minima of the 'data' arise mainly from the dependence on φ of the $\Delta 2\theta$ correction. The values of the optimized parameters, $R_1 = 30$ Å and $(8V_0/V_1)_1 = 4.0$ for the first fitting run, $R_2 = 60$ Å and $(8V_0/V_1)_2 = 3.9$ for the second, are very close to those of the simulated data. Therefore, it is possible to conclude that one can first integrate the rough intensity values in suitable φ intervals and then correct for refraction according to an average φ value. As the data have been simulated with a sample-to-detector distance that is definitely smaller than actual experimental configurations, the good fittings of unsmeared functions demonstrate *a fortiori* that smearing

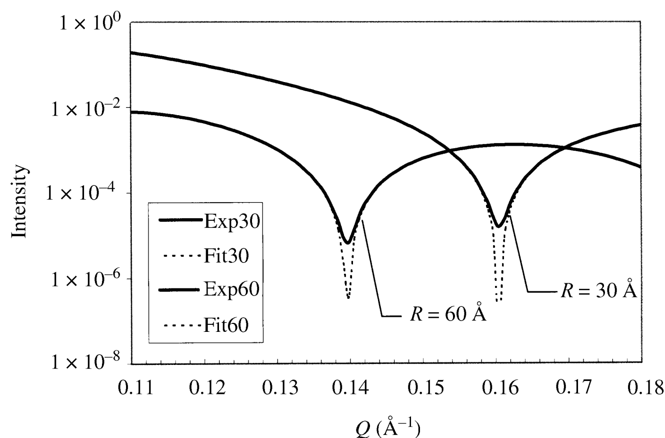

Figure 4
GISAXS intensities of interacting monodispersed hard spheres [equation (11)]. Details around a minimum for the profiles corresponding to hard-sphere radii R = 60 Å and R = 30 Å, respectively, are shown. Exp30 and Exp60 (heavy lines) are the simulated data from equation (11) taking into account sample smearing [equation (9)], refraction and φ integration from $\varphi = 10^\circ$ to $\varphi = 26.5^\circ$. The dashed lines (Fit30 and Fit60) are relative to fitted profiles calculated without sample smearing and taking into account the refraction correction at $\varphi_{av} = 18^\circ$.

effects caused by the size of the illuminated sample area can be neglected in the analysis of GISAXS data.

4. A case study

Equations (5) and (6) give the correction $\Delta 2\theta$ as a function of the experimental parameters (incidence angle α, index of refraction $1 - \delta$, incoming wavelength λ), and of the $(2\theta, \varphi)$ angles. To study how the correction for double refraction affects experimental scattering data, we report here as a case study the analysis of a silica slide sample containing Cu–Ni alloy nanoclusters in a layer, of thickness 100 nm, below the glass surface. The sample was prepared by double implantation of Cu^+ and Ni^+ ions in silica; details of preparation parameters, transmission electron micrographs and procedures for recording the GISAXS pattern of the sample considered here are reported elsewhere (Cattaruzza *et al.*, 2000). While all the angles used for the correction are set out by the scattering geometry with an accuracy that depends on the experimental apparatus, the correction for the index of refraction $1 - \delta$ is calculated from the experimental determination of the critical angle α_c of the composite system. α_c is calculated from the reflectivity curve as the angle corresponding to the half maximum of reflected intensity. The accuracy of its determination depends on the system, as the presence of Kiessig fringes could introduce an uncertainty in the determination. In the present case, the error was found to be around 5%; thus negligible in the following analysis.

In the previously reported study (Cattaruzza *et al.*, 2000), only the scattering data relative to the smallest available φ angle were analysed. According to the simulations reported in the previous section, the experimental intensities are now radially integrated in the range $10 \leq \varphi \leq 26.5^\circ$ and then corrected for refraction according to $\varphi_{av} = 18^\circ$. The integration range is limited to the φ values available for all the relevant 2θ angles, taking into account that recording at $\varphi < 10^\circ$ is hindered by the beam stop, while intensities at $\varphi > 26.5^\circ$ are affected by the Yoneda peak (Yoneda, 1963; Babonneau *et al.*, 1999). The correction for absorption does not produce appreciable effects, owing to the very small thickness of the implanted layer (about 1000 Å).

In Fig. 5, a comparison of the integrated scattered intensity with and without refraction correction is presented (Figs. 5*a* and 5*b*, respectively); fits to the experimental scattering curves are also shown. The model of interacting spherical clusters used for the fitting procedure is based on the local monodisperse approximation [LMA, which assumes complete correlation between particle size and position within the sample (Pedersen, 1994)], on a Weibull-like cluster size distribution and on a Perkus–Yevick structure factor; all these hypotheses are valid for these composites (Cattaruzza *et al.*, 2000).

Fitting parameters are reported in Table 1; the correction for refraction essentially affects the parameters that are involved in the structure factor and are therefore related to the position of the maximum of the scattering curve. In particular, the large decrease in the hard-sphere volume fraction η_{HS} (Pedersen, 1994) is evident; this is caused by the shift of the GISAXS pattern towards smaller scattering angles, which results in the estimation of larger distances between the interacting objects. The difference between η_{HS} = 0.24 reported in Table 1 and η_{HS} = 0.28 previously assessed (Cattaruzza *et al.*, 2000) can be ascribed to the better signal-to-noise ratio achieved by use of the φ integration. As the refraction correction involves a roughly rigid translation of the GISAXS pattern, it is not surprising that the form factor is not concerned very much; indeed, the average radius of the clusters is nearly constant in fitting runs (*a*) and (*b*).

5. Conclusions

The correction for refraction of the incoming beam and of the scattered beam at the sample surface in GISAXS patterns has

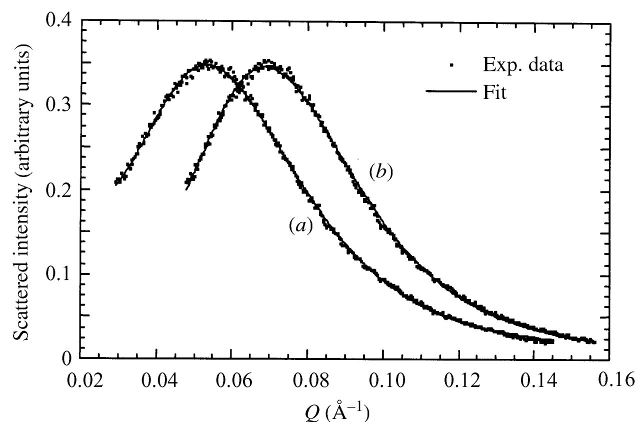

Figure 5
Scattered intensity of Cu^+ + Ni^+ implanted silica obtained by radial integration of the two-dimensional scattering pattern (*a*) with or (*b*) without correction for double refraction of the X-ray beam. Best fitting curves (within the LMA approximation) are also reported.

Table 1
Fitting parameters within the LMA of the scattering curve (*a*) after and (*b*) before correction for double refraction of the X-ray beam impinging on the sample.

η_{HS} is the hard-sphere volume fraction in the structure factor; *a* and *b* are the parameters that define the Weibull function $W(R) = (a/b)(R/b)^{a-1} \exp[-(R/b)^a]$.

Experimental scattering curve	a	b (Å)	Mean cluster radius (Å)	Mean intercluster distance (Å)	η_{HS}
(*a*)	2.48	21.5	19.1	87	0.24
(*b*)	2.35	21.5	21.0	68	0.39

been derived under the assumption of a point-like sample and for an experimental setup consisting of a planar detector perpendicular to the incoming beam. It has been demonstrated by the simulations reported in §3 that the smearing effects arising from the finite size of the illuminated sample are negligible in the small-angle scattering region. The parameters of the simulations are those of a GISAXS experiment previously carried out by the authors (Cattaruzza *et al.*, 2000), but for a shorter sample-to-detector distance, thus ensuring an overestimation of the sample smearing effects. Therefore, equations (5) and (6) can be directly applied to the experimental data to obtain the corrected intensity values.

Furthermore, it has been demonstrated that, whereas for anisotropic implants the correction given by equations (5) and (6) should be applied for each $(2\theta, \varphi)$ pair of angles, for isotropic implants a simplified procedure can be exploited in limited φ ranges, consisting of azimuthal integration of the recorded intensities followed by correction for refraction according to an average φ angle.

References

Acapito, F. d', Thiaudière, D., Zontone, F. & Regnard, J. R. (1998). *Mater. Sci. Forum*, **278–281**, 891–896.
Babonneau, D., Naudon, A., Thiaudière, D. & Lequien, S. (1999). *J. Appl. Cryst.* **32**, 226–233.
Cattaruzza, E., d'Acapito, F., Gonella, F., Longo, A., Martorana, A., Mattei, G., Maurizio, C. & Thiaudière, D. (2000). *J. Appl. Cryst.* **33**, 740–743.
Guinier, A. & Fournet, G. (1955). *Small-Angle Scattering of X-rays*. New York: Wiley.
Kutsch, B., Lyon, O., Schmitt, M., Mennig, M. & Schmidt, H. (1997). *J. Appl. Cryst.* **30**, 948–956.
Levine, J. R., Cohen, J. B., Chung, Y. W. & Georgopoulos, P. (1989). *J. Appl. Cryst.* **22**, 528–532.
Naudon, A. & Thiaudière, D. (1997). *J. Appl. Cryst.* **30**, 822–827.
Pedersen, J. S. (1994). *J. Appl. Cryst.* **27**, 595–608.
Yoneda, Y. (1963). *Phys. Rev.* **131**, 2010–2013.